SCIENCE CHINA Information Sciences



• RESEARCH PAPER •

December 2025, Vol. 68, Iss. 12, 220303:1–220303:21 https://doi.org/10.1007/s11432-025-4639-3

Special Topic: Terahertz Communications for 6G and Beyond: How Far Are We?

Adaptive MAC for space terahertz information network: modeling and performance optimization

Yuanzhi HE^{1,2*}, Zhiqin CAO¹, Xiang CHEN¹ & Xingyang WANG²

¹School of Systems Science and Engineering, Sun Yat-sen University, Guangzhou 510275, China
²A Research Institute of the PLA Information Support Force, Beijing 100141, China

Received 14 May 2025/Revised 22 August 2025/Accepted 17 October 2025/Published online 18 November 2025

Abstract The space terahertz information network (STIN) leverages the terahertz (THz) frequency band for data transmission, offering advantages of large capacity and high-speed communication. However, existing research commonly overlooks the profound impact of THz-specific characteristics on the performance of the satellite network's medium access control (MAC) layer and lacks adaptive MAC mechanisms that can fully match THz's high-speed transmission capabilities. To address this issue, this paper proposes an adaptive MAC scheme customized for STIN. This scheme integrates information from the physical, link and network layers, dynamically adjusting the THz beamwidth and timeslot allocation during each transmission cycle, and selecting the optimal handshake procedure and the MAC access mechanism based on varying traffic loads and channel conditions. The main innovations of this paper are as follows. First, an STIN MAC performance analysis framework combining queuing theory and geometric probability models is established, systematically revealing the constraints imposed by THz characteristics on MAC performance. Second, a multi-parameter cooperative optimization MAC mechanism is proposed, which can significantly improve throughput and link resource utilization in complex dynamic environments. Using terahertz communication between GEO satellites and LEO constellations as a typical scenario, simulations are conducted, and the results show that the proposed scheme achieves up to 27% throughput gain under link fluctuation conditions compared with traditional MAC mechanisms, fully verifying its engineering application potential.

Keywords terahertz, satellite network, MAC, performance optimization, modeling

Citation He Y Z, Cao Z Q, Chen X, et al. Adaptive MAC for space terahertz information network: modeling and performance optimization. Sci China Inf Sci, 2025, 68(12): 220303, https://doi.org/10.1007/s11432-025-4639-3

1 Introduction

6th generation mobile network (6G) demands higher network reliability and greater coverage, which makes research on the 6G space segment particularly critical. As an information transmission network connecting the ground, air and space, the space information network is expected to play a key role in the 6G era [1, 2]. 6G communications are anticipated to break through the limitations of millimeter waves. They are expected to extend into the terahertz (THz) frequency band to achieve ultra-high-speed and ultra-large-bandwidth transmission. The terahertz band remains one of the least explored regions of the electromagnetic spectrum, primarily due to the lack of efficient and practical THz transceivers and antennas. However, significant advances in semiconductor technologies and new materials in recent decades have made practical THz communication systems increasingly feasible [3–6].

The space terahertz information network (STIN) establishes a multilayer integrated network by deploying THz links among high, medium, and low Earth orbit (LEO) satellites, as well as near-space platforms. These links include inter-satellite THz links, inter-constellation THz links, and THz access links. Due to the high attenuation characteristics of THz waves, highly directional multi-beam phased array antennas (MBPAA) are utilized to overcome significant path losses while enabling flexible network communication, supporting the needs for high-speed and low-latency transmission [7].

In the non-terrestrial network (NTN) architecture, geostationary Earth orbit (GEO)-LEO cooperative communication is a key component for achieving global coverage and high-capacity relaying. It has been repeatedly emphasized in both the ITU World Radiocommunication Conference and the 3GPP NTN study items [8, 9]. Typical applications include global wide-area coverage, relay transmission for deep

^{*} Corresponding author (email: he_yuanzhi@126.com)

space telemetry and control missions, and multi-layer cooperative information transmission across the ground-LEO-GEO hierarchy. GEO nodes offer strong scheduling and relay capabilities, while LEO nodes provide low-latency and high-frequency link establishment. Therefore, the GEO-LEO link is not only a critical element of the NTN architecture, but also represents the boundary challenge for terahertz communication under highly dynamic, long-distance, and strong Doppler scenarios. It serves as a representative application scenario for studying novel MAC mechanisms and link control strategies.

Medium access control (MAC) is a critical component in ensuring network performance. Traditional MAC protocols may encounter performance bottlenecks when handling THz characteristics, such as high attenuation, large bandwidth, and short frame lengths. Therefore, it is necessary to redesign MAC mechanisms considering THz-specific properties to achieve higher performance and access efficiency.

Current literature on THz communication network access control mainly focuses on several aspects. These include the impacts of THz channel characteristics, the use of directional antennas, the short frame lengths caused by high frequencies, and the influence of large bandwidths on MAC performance. On one hand, MAC design must consider THz channel properties such as transmission windows [10], losses [11,12], and interference [13]. On the other hand, the use of highly directional THz antennas introduces new challenges for MAC, including beam scanning [14], alignment [15], tracking [16], synchronization [17], and relay node selection [18]. Meanwhile, the short frame lengths caused by the high frequency of THz waves exacerbate scheduling and overhead issues, necessitating a performance balance among frame structure, channel characteristics, and link quality [19].

These requirements are particularly challenging due to the high frequency, strong directionality, and strong dependence on line-of-sight (LoS) transmission inherent to THz communications. Beam scanning must rapidly search over a wide angular range to find the optimal direction for initial access or reconnection. However, the narrow beamwidth and high-dimensional search space result in significantly increased overhead. Beam alignment is critical during the establishment and maintenance of communication links, even minor node movements or changes in orientation may lead to link disruption, necessitating frequent directional adjustments and increasing protocol complexity. Beam tracking further requires the MAC layer to continuously monitor and adjust beam directions to maintain a stable connection, which becomes particularly challenging in high-speed or dynamic scenarios. In terms of synchronization, high-frequency communications are extremely sensitive to clock offsets and signal misalignments, making traditional synchronization mechanisms inadequate and requiring the design of highly precise solutions. Relay node selection is constrained by the high directionality and severe path loss of THz signals. Communication opportunities between nodes are limited, necessitating joint decisions based on spatial location, link quality, and beam status, thereby increasing the complexity of scheduling algorithms. The beam status refers to the key attributes of a communication beam at a specific time, including beam direction (pointing angle) and beamwidth (coverage area). These factors directly affect link availability and link duration, thereby exerting a significant impact on access control and resource scheduling.

These challenges collectively imply that MAC design for THz communications must possess enhanced sensing, decision-making, and control capabilities to address the multidimensional optimization demands of dynamic environments. In other words, the physical-layer characteristics of high frequency, high directivity, and link volatility directly shape the design objectives of the MAC layer. The MAC mechanism is not only required to avoid access collisions, but also to perceive and adaptively optimize beam status, link quality, and scheduling strategies, thereby enabling cross-layer coordination.

Ref. [20] proposed the multiple angular division multiplexing (MA-ADM) protocol, a THz MAC mechanism based on angle-division multiplexing, which introduces an auxiliary storage mechanism to reduce beam alignment overhead in highly directional communications, and enhances multi-user concurrent transmission capability through angular partitioning. Ref. [21] designed the adaptive directional antenna protocol (ADAPT) protocol, which utilizes a dynamic adjustment mechanism for directional antennas to address the challenges of beam alignment and collision detection in THz communications, enabling adaptive switching of the MAC layer across different communication directions. Ref. [22] investigated a dual intelligent reflecting surface (IRS) assisted broadband THz communication system, analyzed its performance, and optimized the reflective surface configuration parameters, providing theoretical support for reflection-enhanced mechanisms in future THz communication environments. Furthermore, the advantages of using artificial intelligence to solve access control problems have been widely recognized, with an increasing amount of related research. Ref. [23] targeted highly dynamic aerial networks and introduced an intelligent MAC mechanism that integrates multidimensional information such as modulation schemes, beam direction, frequency, and power. Through cross-layer optimization and artificial intelligence (AI)

algorithms, it improves access control efficiency in high-frequency, high-speed environments.

From the above discussion, it is evident that STIN MAC protocol design does not need to overly emphasize collision avoidance in channel access. Instead, the key lies in efficiently coordinating satellites for dynamic line-of-sight communication to meet STIN's requirements for large-capacity and high-speed transmission. The existing research faces the following shortcomings.

- (1) Insufficient consideration of the impact of THz characteristics on satellite network MAC performance, including the influence of THz ultra-large bandwidth on timeslot size, and the impact of THz beamwidth on antenna gain and the number of LEO nodes within coverage.
- (2) The ultra-large bandwidth of THz further exacerbates the low channel utilization and high overhead problems in satellite network MAC scheduling and transmission. To meet the requirements for large-capacity and efficient transmission and to match THz's high-speed capabilities, adopting an adaptive hybrid MAC mechanism is an effective solution. However, there is currently a lack of research on adaptive hybrid MAC mechanisms for STIN.

This paper addresses the existing issues in current designs and conducts research on STIN MAC mechanisms. Firstly, based on queuing theory and geometric probability models, a theoretical model for STIN MAC performance analysis is constructed. It systematically analyzes the impact of THz characteristics on MAC layer performance, including the effects of THz ultra-large bandwidth, beam constraints, and long propagation delays on timeslot design, link reliability, and channel scheduling efficiency. On this basis, a cross-layer collaborative adaptive MAC scheme is designed. This scheme integrates information from the physical, link, and network layers. It dynamically adjusts the THz beamwidth and timeslot length during each transmission cycle, and selects the optimal handshake procedure and access mechanism according to network load and channel quality. In this way, it matches the high-speed transmission capabilities of THz communications and adapts to the high dynamics of the space environment. Extensive simulation experiments were conducted using THz communication between the GEO satellite and the LEO constellation as the application scenario. The results validate the effectiveness and robustness of the proposed theoretical model and adaptive mechanism. The main contributions of this paper are summarized as follows.

- (1) A theoretical model for STIN MAC based on queuing theory and geometric probability analysis is constructed. An explicit expression for network throughput is derived, and the comprehensive impact of factors such as network load, packet size, number of LEO nodes, and long propagation delays on MAC performance is quantitatively analyzed. This reveals the performance trade-offs between random access and fixed allocation mechanisms, providing a theoretical basis for key mechanisms such as packet aggregation, sliding windows, and flow control.
- (2) An adaptive MAC mechanism tailored for STIN is proposed, capable of dynamically optimizing beamwidth and timeslot length and selecting the optimal handshake method and access strategy in each transmission cycle. Under beamwidth constraints, the mechanism can find the best beamwidth design and MAC method, effectively improving channel utilization and transmission efficiency, and significantly enhancing the MAC layer's adaptability to complex space environments.
- (3) Simulation was conducted using the THz communication between the GEO satellite and the LEO constellation as a case study, and the results verify the effectiveness of the theoretical analysis model. Through extensive experiments, the design patterns and differentiated features of the STIN MAC mechanism are revealed, and the robustness of the adaptive MAC mechanism in coping with complex and variable space environments is confirmed. This result highlights the engineering value and application prospects of the study.

The remainder of this paper is organized as follows. Section 2 provides a detailed introduction to the system model. Section 3 elaborates on the problem and proposes the STIN adaptive MAC scheme. Sections 4 and 5 construct the STIN MAC analysis model and derive network throughput, followed by an analysis of the effects of different variables on MAC performance. Section 6 conducts simulations and discusses the results. Finally, Section 7 summarizes the main findings.

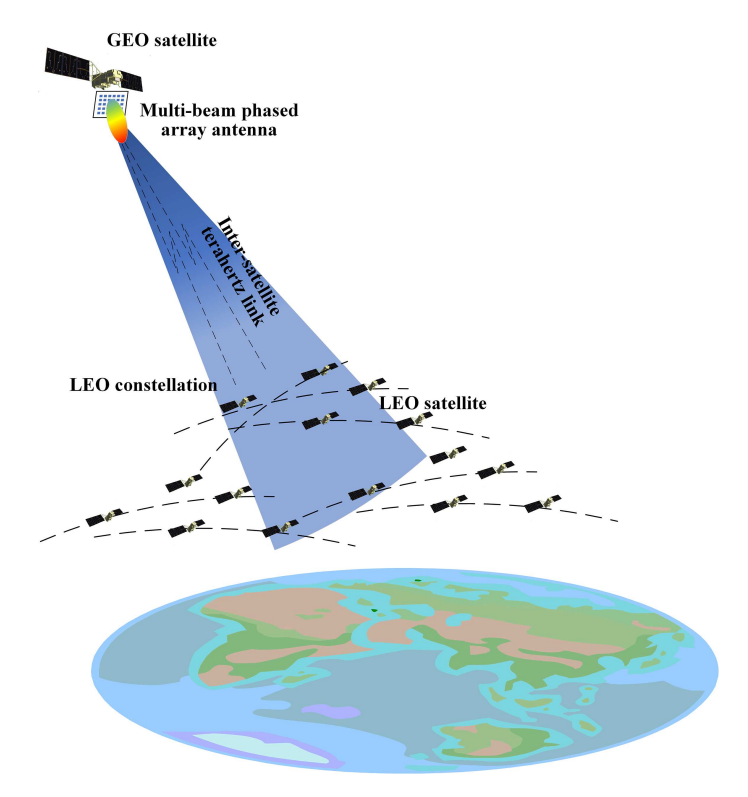


Figure 1 (Color online) Communication scenario between GEO and LEO constellations.

2 System model

2.1 System architecture

Considering the communication scenario between GEO and LEO constellations in STIN, the GEO satellite utilizes a multi-beam phased array antenna to form THz beams, covering multiple LEO satellites for uplink communication, with the GEO acting as the receiver initiating the communication, as illustrated in Figure 1. It is assumed that the packet arrivals follow a Poisson process, and the collision model is assumed such that one packet transmission is successful only when there are no concurrent transmissions.

2.2 Handshake methods

During the access control process between GEO and LEO satellites, the initial access considers two handshake methods initiated by the receiver: a 1-way handshake and a 3-way handshake [21].

Although the GEO and LEO satellites can compute their relative positions based on orbital data, factors such as orbit prediction errors, high-speed satellite movement, and dynamic beam scanning errors may still lead to a "deafness" problem. By adopting a receiver-initiated communication design, the receiver can provide feedback to the sender, enabling beam direction adjustments to mitigate the deafness issue.

In the 3-way handshake process initiated by the receiver, the GEO satellite, acting as the receiving node, periodically broadcasts a call-to-action (CTA) packet to notify LEO satellites that communication can begin. If a LEO satellite has data to transmit, it responds with a request-to-send (RTS) packet. Upon receiving the RTS, the GEO satellite grants access to the channel by sending a clear-to-send (CTS) packet, thereby completing the 3-way handshake. Upon receiving the CTS, the LEO satellite transmits the data according to the preset MAC policy. After successfully receiving the data, the GEO satellite sends an ACK message. The handshake process is illustrated in Figure 2.

In the 1-way handshake process initiated by the receiver, the CTA-RTS packet exchange is omitted. Instead, the GEO satellite periodically broadcasts a CTS packet, announcing its availability to the LEO satellites. Upon receiving a CTS, the LEO satellites wait for a random back-off time before beginning data transmission according to the preset MAC policy. The handshake process is illustrated in Figure 3.

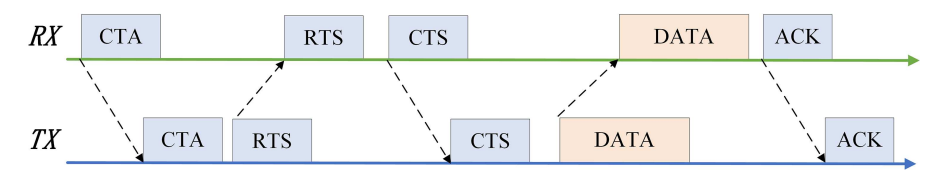


Figure 2 (Color online) Receiver-initiated 3-way handshake.

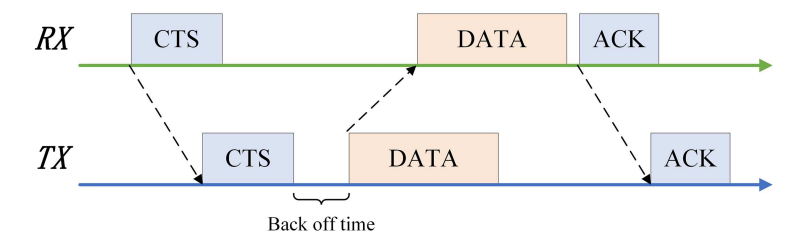


Figure 3 (Color online) Receiver-initiated 1-way handshake.

The purpose of setting a random back-off time is to address the collision problem that may arise when multiple LEO satellites receive the same CTS simultaneously and attempt to transmit data immediately. By introducing a brief and random waiting period before transmission, the probability of packet collisions is reduced, enabling fairer and more efficient channel access.

The differences between the two handshake methods primarily lie in two aspects: the information exchanged during the handshake and the resulting overhead. In the 3-way handshake, multiple interactions synchronize the link and resource allocation. In contrast, under the 1-way handshake, LEO satellites cannot exchange resource allocation information with the GEO satellite. Through the 3-way handshake, resource allocation in the MAC process can be dynamically adjusted, such as dynamically adjusting the number of time division multiple access (TDMA) timeslots based on the received RTS messages.

On the other hand, the overhead of the receiver-initiated 3-way handshake is the sum of the collision retransmission overhead and the handshake access overhead. In the 3-way handshake method, collisions occur due to RTS packet collisions. The initial random access success is modeled as a geometric distribution event, with an expected value of $\frac{1}{P_{\text{success}}}$, indicating that an average of $\frac{1}{P_{\text{success}}}$ attempts are needed to achieve successful access, meaning that the number of collisions is $\frac{1}{P_{\text{success}}} - 1$. Thus, the total overhead of the 3-way handshake is given by

$$O_{3-\text{way}} = \left(\frac{1}{P_{\text{success}}} - 1\right) \cdot \left(T_{\text{RTS}} + T_{\text{CTS}} + 2T_P\right) + \left(T_{\text{CTA}} + T_{\text{RTS}} + T_{\text{CTS}} + 3T_P\right),\tag{1}$$

where $T_{\rm RTS} + T_{\rm CTS} + 2T_P$ represents the random access timeout duration. If a terminal does not receive a response after transmitting data and the timeout period expires, it assumes that a collision has occurred and retransmits the data. In contrast, the receiver-initiated 1-way handshake does not incur collision retransmission overhead, so the overhead is simply $O_{1\text{-way}} = T_{\rm CTS} + T_P$. $P_{\rm success}$ denotes the success probability of random access, and $T_{\rm RTS}$, $T_{\rm CTA}$, and $T_{\rm CTS}$ represent the transmission delays of the control messages during the handshake process, while T_P represents the propagation delay.

2.3 MAC mechanisms

Random access control schemes (such as Aloha) and fixed allocation access control schemes (such as TDMA) each have their own advantages and applicable scenarios. Under low traffic loads, random access control schemes perform better in terms of delay and throughput. However, as the traffic load increases, the probability of collisions in random access rises, leading to higher retransmission overhead, whereas fixed allocation access can fully utilize the channel and enhance throughput.

To meet the large-capacity and high-efficiency transmission requirements of STIN, adopting an adaptive hybrid MAC mechanism is an effective solution. This study considers the design of an adaptive mechanism between random MAC and fixed MAC mechanisms, including Aloha, Slotted ALOHA (S-Aloha), and TDMA. Aloha is a random access protocol in which nodes can transmit data at any time. While the mechanism is simple, it suffers from a high probability of collisions. S-Aloha improves upon Aloha by introducing a timeslot structure, allowing nodes to transmit only at the beginning of a slot. This effectively

halves the collision probability and improves channel utilization. In contrast, TDMA adopts a centralized scheduling approach, dividing time into multiple slots and assigning them to individual nodes, thereby avoiding collisions. It is well-suited for scenarios with stable links and high synchronization accuracy. Each of these protocols has its own advantages and is applicable to different access control requirements under varying link conditions and network densities.

Combinations of different MAC mechanisms and handshake methods are considered, including the following.

- 3way-TDMA. A 3-way handshake with TDMA scheduling that can dynamically adjust the number of slots.
 - 1way-TDMA. A 1-way handshake with fixed TDMA resource allocation.
- 1way-S-Aloha/Aloha. A 1-way handshake in receiver-initiated communication based on S-Aloha/Aloha.

In this paper, the handshake mechanism refers to the process of link access and scheduling parameter negotiation, and is not limited to contention-based MAC protocols. Even in TDMA mechanisms, in order to support adaptive resource allocation and link state confirmation, handshake procedures can be used to achieve more refined scheduling control. In 3way-TDMA, the 3-way handshake includes an access request (RTS), a scheduling response (CTS), and a transmission confirmation (ACK/CTA), which enables the dynamic adjustment of the number of allocated slots before transmission according to real-time load and channel conditions, thereby improving the adaptability and channel utilization of TDMA in time-varying networks. In contrast, 1way-TDMA only performs a single resource confirmation before transmission and cannot adjust the number of slots during transmission. Similarly, in 1way-S-Aloha and Aloha protocols, the handshake is mainly used for communication request initiation and random access collision detection. In this paper, handshake procedures are combined with TDMA mechanisms in modeling to achieve flexible adjustment of access confirmation and resource allocation in space terahertz networks with dynamic load and varying link conditions, thereby combining the efficiency of TDMA with adaptability in dynamic environments.

2.4 Communication procedures

This study focuses on the transceiver process over a single channel in the GEO-LEO constellation communication scenario. After accessing the channel, each LEO satellite begins data transmission. The communication procedure is illustrated in Figure 4.

We further analyze the impact of mobility in the GEO-LEO scenario. The maximum radial velocity of the GEO-LEO inter-satellite link is approximately ± 3.1 km/s, corresponding to a Doppler shift of about 3.1 MHz at a carrier frequency of 0.3 THz. The coherence time is about 0.14 μ s, which is far shorter than the configured time slot length. Therefore, its impact can be effectively eliminated by frequency offset estimation and tracking at the physical layer. The beam scanning rate required for narrow-beam communication is around 0.01°/s, which can be supported by modern phased array technology. Hence, the impact of mobility on link performance is minor and does not affect the main conclusions. Since this paper focuses on the performance optimization of adaptive MAC mechanisms under different network load and channel conditions, the impact of mobility can be further mitigated in practical systems by designing reasonable switching periods and applying pre-configuration mechanisms.

2.5 Channel model

For simplification, the channel model between GEO and LEO satellites is based on the free-space propagation loss model under the assumption of an ideal vacuum environment,

$$L_{fs} = 20 \log \left(\frac{4\pi df}{c} \right). \tag{2}$$

The effect of molecular absorption on noise is ignored, and only thermal noise is considered,

$$N = 10\log(k_B T_{\text{sys}} B) + 30, (3)$$

where d denotes the distance between the GEO and LEO satellites, f is the THz operating frequency, c is the speed of electromagnetic waves in the medium, k_B is the Boltzmann constant, $T_{\rm sys}$ is the system temperature, and B is the operating bandwidth.

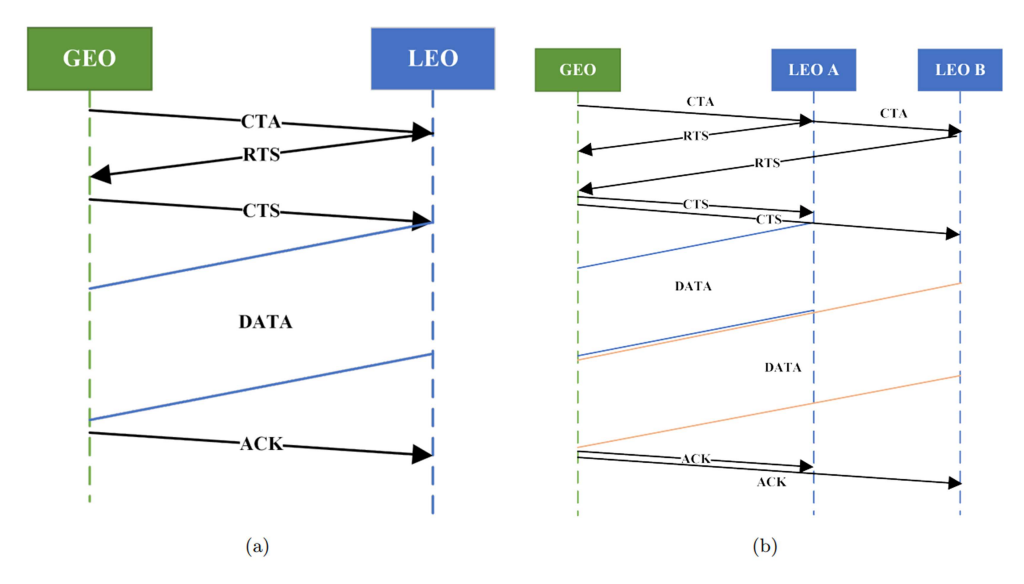


Figure 4 (Color online) (a) Packet transmission process with 3-way handshake for a single LEO; (b) packet transmission process with 3-way handshake for multiple LEOs.

The GEO-LEO inter-satellite link studied is entirely located in the rarefied upper atmosphere, where the signal does not traverse the troposphere or most of the stratosphere. Thus, atmospheric molecular absorption, rain attenuation, and cloud and fog attenuation can be neglected. According to ITU-R P.676, at a frequency of 0.3 THz and altitudes above 30 km, the specific attenuation is below 10^{-5} dB/km. For a near-ground segment of 50 km, the total absorption loss is less than 0.01 dB, which is negligible compared with the free-space path loss of approximately 233 dB over the 36000 km transmission distance. Therefore, adopting the free-space path loss model can accurately capture the main attenuation characteristics of GEO-LEO terahertz links. Additional attenuation factors such as pointing errors and hardware insertion losses would cause a certain reduction of link margin in engineering practice, but their effects are constant-scale degradations and do not change the relative performance comparison and conclusions of different MAC mechanisms. This paper focuses on analyzing the potential performance upper bound of mechanism design, and these additional attenuation terms are not considered for simplification.

2.6 Antenna model

The antenna gains and the 3 dB beamwidth are considered independent of distance. The directional gain of a highly directional antenna can be approximated as

$$G_a \approx 10\log\left(\frac{4\pi}{\Omega_A}\right) \approx 10\log\left(\frac{4\pi}{\theta_h\phi_h}\right),$$
 (4)

where Ω_A represents the physical beam angle of the antenna array, θ_h and ϕ_h represent the half power beam widths (HPBW) in the elevation and azimuth planes, respectively. Assuming that the HPBWs in both planes are the same, i.e., $\theta_h = \phi_h = \theta$, then

$$G_a \approx 10\log\left(\frac{4\pi}{\theta^2}\right).$$
 (5)

The GEO satellite utilizes a multi-beam phased array antenna, forming multiple narrow beams with a large number of array elements to achieve wide-area spatial coverage [24,25].

2.7 Demodulation threshold

The received signal strength must exceed the reception power threshold. The received signal power P_r is

$$P_r = P_t + G_t + G_r - L_{fs}. (6)$$

The signal-to-noise ratio (SNR) is

$$SNR = P_r - N. (7)$$

Thus, the following condition must be satisfied:

$$SNR \geqslant SNR_{min},$$
 (8)

where SNR_{min} denotes the demodulation threshold, which is related to the modulation and coding scheme as well as the bit error rate requirements. G_t is the transmit antenna gain, G_r is the receive antenna gain, L_{fs} is the path loss, and N is the noise power.

2.8 Retransmission probability

In the communication process between GEO and LEO satellites, two situations are considered for retransmissions: one caused by packet collisions, and the other caused by erroneous packets. The collision model assumes that when concurrent transmissions occur, packet collisions happen, requiring retransmissions. Retransmissions due to erroneous packets are characterized by the packet error rate (PER).

3 STIN adaptive MAC scheme

3.1 Problem description

The characteristics of THz communication directly impact the MAC layer performance of satellite networks, potentially leading to performance bottlenecks. On one hand, the ultra-high data transmission rate significantly shortens the symbol period at the physical layer, thereby reducing the time required for transmitting a minimum transmission unit, namely the timeslot length, and resulting in an extremely fine-grained slot structure. Such fine granularity increases the proportion of control overhead, exacerbating the problem of low channel utilization. Although increasing the packet size can improve channel utilization, it also leads to higher retransmission overhead. On the other hand, the THz beamwidth affects both the antenna gain and the number of LEO nodes within the coverage area. While ensuring sufficient antenna gain to meet the demodulation threshold requirements, it is also necessary to consider the impact of the number of LEO nodes within the beamwidth θ coverage area on MAC performance [26].

Meanwhile, in traditional MAC schemes, random access control schemes (such as S-Aloha) and fixed allocation access control schemes (such as TDMA) each have their own advantages and applicable scenarios.

However, both random access and fixed allocation schemes fall short of fully matching the high-speed transmission capabilities of THz communications, especially in dynamic space environments where link quality is unstable and traffic load fluctuates significantly. In such cases, an adaptive hybrid MAC scheme is required to manage and optimize performance.

In summary, the MAC mechanism is required to perceive and collaboratively adapt to the variations of space terahertz links across multiple dimensions, including traffic load, spatial coverage, and timeslot scheduling. This enables the joint optimization and regulation of access control strategies, beam parameters, frame structure, and timeslot allocation, thereby improving resource utilization efficiency and task completion performance.

3.2 Multi-dimensional cooperative adaptive MAC mechanism

Based on the above problem analysis, this section proposes a multi-dimensional cooperative adaptive MAC mechanism (MCTA-MAC) for STIN. This mechanism comprehensively considers beamforming gain and line-of-sight coverage at the physical layer, SNR at the link layer, and traffic scheduling demands at the network layer. It is designed from two aspects: (i) collaborative optimization of access control strategies with multiple parameters, and (ii) dynamic allocation of frame structure and timeslots. The aim is to improve channel utilization, match the ultra-high-speed transmission capability of terahertz communications, and adapt to unstable link quality, highly fluctuating traffic loads, and diverse mission requirements.

Unlike traditional MAC mechanisms, the core idea of the adaptive MAC mechanism lies in dynamically selecting the optimal access mode and parameter configuration according to the current network state (e.g., link quality, traffic load). This enables joint adaptive optimization of MAC mechanism type, handshake procedure, beamwidth, and timeslot allocation. The MCTA-MAC framework is shown in Figure 5.

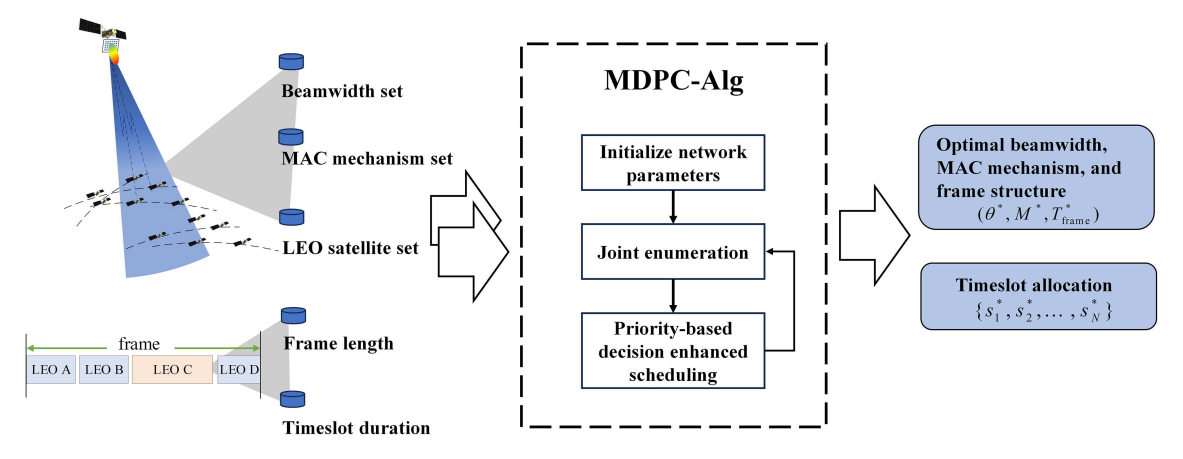


Figure 5 (Color online) Framework of the MCTA-MAC mechanism.

3.2.1 Joint parameter adaptive control

The JPAC mechanism aims to flexibly switch among multiple representative access mechanisms (TDMA and ALOHA) and handshake methods (1-way and 3-way handshakes), in order to adapt to varying link states and traffic characteristics. In the MAC decision-making process, a multi-factor decision model based on link SNR, network load, node distribution density, and data volume is employed to jointly optimize beamwidth, handshake mode, and MAC type. Within the feasible beamwidth range constrained by link demodulation thresholds, the beamwidth is dynamically adjusted. The decision algorithm evaluates the throughput performance of three candidate mechanisms: 3way-TDMA, 1way-TDMA, and 1way-S-Aloha, under different conditions, and selects the optimal combination of beamwidth, handshake procedure, and MAC type to achieve adaptive optimization.

According to the constraint that the received SNR must exceed the minimum threshold i.e., SNR \geqslant SNR_{min}, the constraint range of the THz beamwidth θ can be derived. The single-beam antenna gain is approximated as $G_0 \approx 10 \log_{10} \left(\frac{4\pi}{\theta_0^2}\right)$. Assuming that the antenna gains of the transmitter and receiver remain constant within the 3 dB frequency window and are equal, i.e., $G_t = G_r = G_0$, the expected antenna gain can be expressed as $G_0 \geqslant \frac{\text{SNR}_{\min} + N + L_{fs} - P_t}{2}$. Therefore, the THz beamwidth θ_0 is given by

$$\theta_0 \leqslant \sqrt{\frac{4\pi}{10^{(\text{SNR}_{\min}+N+L_{fs}-P_t)/20}}},\tag{9}$$

where SNR_{min} denotes the minimum required received SNR, N is the noise power, L_{fs} is the free-space path loss, and P_t is the transmit power.

When a GEO satellite employs a multi-beam phased-array antenna, multiple narrow beams can be formed by combining a large number of array elements, thereby achieving wide-area coverage. The resulting beam coverage angle can be expressed as $\theta_B \approx \theta_0 \cdot N_{\text{beam}}$, where θ_0 is the beamwidth of a single array element, and N_{beam} is the number of synthesized beams. Thus, under link constraints, the feasible range of THz beamwidth is $\theta \in [\theta_0, N_{\text{beam}} \cdot \theta_0]$.

The JPAC mechanism dynamically selects a candidate beamwidth θ within the allowed interval $[\theta_0, N_{\text{beam}} \cdot \theta_0]$, monitors the link noise power N during each transmission cycle, and determines the network load G and packet volume L_{req} under the corresponding beamwidth. It then evaluates the throughput performance of three candidate MAC mechanisms: 3way-TDMA, 1way-TDMA, and 1way-S-Aloha, denoted as $S(m, G(\theta))$, and finally selects the parameter pair (θ^*, m^*) that maximizes throughput. In this process, both the beamwidth and the handshake/MAC type are adaptively optimized in a joint manner, enabling coordinated adaptation to both link state and traffic dynamics. Here, the network load is defined as $G = N_{\text{LEO}} \cdot q$, where N_{LEO} is the number of LEO satellites covered by the beam, and q is the average packet arrival probability of each LEO satellite. The set of candidate MAC types is $m \in \{3\text{way-TDMA}, 1\text{way-TDMA}, 1\text{way-S-Aloha}\}$.

The throughput model $S(m, G(\theta))$ is a function of beamwidth θ and the selected MAC type m, while the network load $G(\theta)$ is a function of beamwidth, reflecting the trade-off between link coverage and collision probability. The MAC mechanism itself defines the access strategy (e.g., the dedicated slots of TDMA vs. the contention-based access of S-Aloha), and together with the selected beamwidth and

access method, determines the efficiency of resource utilization and the overhead of handshake signaling, which in turn significantly influence overall system performance.

In summary, the JPAC mechanism determines the optimal beamwidth θ^* and MAC mode m^* by solving the throughput maximization problem max $S(m, G(\theta))$, thereby achieving adaptive control that accounts for both varying link states and dynamic traffic loads. This optimization model not only captures the coupling relationship between physical-layer link conditions and MAC-layer design, but also provides a continuous optimization framework for subsequent performance analysis and theoretical validation. The specific optimization process is presented in Section 4.

3.2.2 Slot-pipelined and variable frame scheduling

To address the issue of high bandwidth utilization in terahertz communications leading to small slot granularity, resource fragmentation, and significant overhead, the proposed MCTA-MAC introduces a joint adjustment mechanism. Specifically, according to the current network load and packet size, the frame length is adaptively adjusted, and each terminal is allocated a continuous slot window. This enables multi-packet pipelined transmission, reduces handshake overhead, aligns with varying traffic demands, and ultimately improves channel utilization.

Assume that the number of LEO satellite nodes within the coverage area of the THz beam is n. The required number of continuous timeslots allocated to each LEO node according to its data transmission demand can be expressed as $N_{\rm slot} = \left\lceil \frac{L_{\rm req}}{r \cdot T_{\rm slot}} \right\rceil$, where $L_{\rm req}$ denotes the amount of data to be transmitted, r is the link transmission rate, and $T_{\rm slot}$ is the duration of a single timeslot. The total frame length for one transmission cycle is then given by $T_{\rm frame} = \sum_{i=1}^n N_{\rm slot}^{(i)}$, where $N_{\rm slot}^{(i)}$ denotes the number of timeslots allocated to the i-th LEO node.

3.3 Multi-dimensional parameter cooperative scheduling algorithm

Considering that the above mechanisms involve multiple parameter combinations and large search spaces, this paper proposes a multi-dimensional parameter cooperative scheduling algorithm (MDPC-Alg) to enhance candidate selection efficiency through coordinated parameter adjustment. The core idea is as shown in Algorithm 1. First, all feasible parameter combinations are jointly enumerated, including all possible beamwidth values $\theta \in \Theta$ and MAC mechanisms $m \in \mathcal{M}$. Second, a pruning mechanism based on a performance lower bound is introduced to rapidly eliminate parameter combinations that cannot satisfy the minimum system performance threshold, thereby improving computational efficiency. Third, continuous timeslot windows are allocated for each terminal according to its data transmission demand and the link transmission rate, thus enabling efficient resource scheduling. Finally, a throughput calculation model is established to identify the parameter combination that maximizes system performance.

This algorithm not only retains the globality of joint search but also incorporates a pruning mechanism based on performance lower bounds, thereby achieving a structured and efficient multi-parameter joint optimization capability.

4 STIN MAC analysis model

For the uplink communication scenario of receiver-initiated communication, where a GEO satellite employs a multi-beam phased-array antenna to form THz beams covering LEO satellites, a theoretical analysis model of the STIN adaptive MAC mechanism is constructed. The model is developed based on queuing theory and geometric probability, while incorporating the unique characteristics of THz communications, to describe the initial access process and the MAC scheduling transmission in the GEO-LEO communication scenario.

4.1 Collision rate of MAC mechanisms

For the convenience of theoretical modeling and analysis, we make the following assumptions when constructing the theoretical analysis model of the STIN adaptive MAC mechanism: (1) the packet arrivals of each node follow a Bernoulli process; (2) the transmission distance from all terminals to the access node is identical; (3) a single-receiver, single-channel access model is considered, where all system parameters

Algorithm 1 Multi-dimensional parameter cooperative scheduling algorithm (MDPC-Alg).

Require: Terminal set $\{L_i, r_i, b_i\}$, beamwidth set Θ , MAC mechanism set $M = \{3$ way-TDMA, 1way-TDMA, 1way-S-Aloha $\}$, times lot length $T_{\rm slot},$ performance lower-bound coefficient $\alpha.$ **Ensure:** Optimal parameter combination (θ^*, m^*) , timeslot allocation scheme $\{s_1^*, s_2^*, \dots, s_n^*\}$. 1: Initialize maximum throughput $S_{\text{max}} \leftarrow 0$; 2: for each $\theta \in \Theta$ do for each $m \in M$ do Compute throughput lower bound $S_{\text{th}} \leftarrow \alpha \cdot S$; 4: if $S(m, G(\theta)) < S_{th}$ then 6: continue; 7: end if 8: for each terminal $i \in [1, n]$ do Compute required timeslot allocation: $N_{\text{slot}} \leftarrow \left\lceil \frac{L_{\text{data}}}{r \cdot T_{\text{slot}}} \right\rceil$; 9: 10: Compute throughput of current parameter set $S(m, G(\theta))$; 11: 12: if $S > S_{\max}$ then Update optimal solution: $(\theta^*, m^*, \{s_i^*\}) \leftarrow (\theta, m, \{s_i\});$ 13: 14: $S_{\max} \leftarrow S;$ 15: 16: end for 17: end for 18: **return** Optimal combination $(\theta^*, m^*, \{s_i^*\})$.

are consistent, including channel model, beam configuration, and transmission probability; (4) in the collision model, if no concurrent transmission occurs, a packet is successfully delivered.

The adaptive MAC scheme dynamically adjusts among multiple MAC mechanisms, including Aloha, S-Aloha, and TDMA. To evaluate the performance of different MAC mechanisms under the above assumptions, we derive the slot utilization states based on probabilistic analysis, namely success probability, idle probability, and collision probability. Accordingly, the following results are obtained.

For the Aloha mechanism, the success probability is given by $P_{s,\text{Aloha}} = Ge^{-2G}$, the idle probability is $P_{i,\text{Aloha}} = e^{-2G}$, and the collision probability is $P_{c,\text{Aloha}} = 1 - e^{-G} - Ge^{-2G}$. For the S-Aloha mechanism, the success probability is $P_{s,\text{S-Aloha}} = Ge^{-G}$, the idle probability is $P_{i,\text{S-Aloha}} = e^{-G}$, and the collision probability is $P_{c,\text{S-Aloha}} = 1 - e^{-G} - Ge^{-G}$. For the TDMA mechanism, since collisions do not occur, the success probability is $P_{s,\text{TDMA}} = 1$, the idle probability is $P_{i,\text{TDMA}} = 0$, and the collision probability is $P_{c,\text{TDMA}} = 0$. Here, the traffic load is denoted by $G = N_{\text{LEO}} \cdot q$, where N_{LEO} represents the number of LEO satellites within the beam coverage, and q is the probability of packet transmission at each LEO satellite.

4.2 Overhead of handshake methods

In the communication process between GEO and LEO satellites, two types of retransmissions are considered: one caused by packet collisions and the other caused by erroneous packets. The retransmission probability is $P_{\text{retrans}} = 1 - P_s(1 - \text{PER})$, where P_s denotes the successful packet transmission probability for each MAC mechanism, and PER denotes the packet error rate. Thus, considering the packet error rate, the probability of successful packet transmission is $P_{\text{success}} = P_s(1 - \text{PER})$.

The overhead of the receiver-initiated 3-way handshake is the sum of the collision retransmission overhead and the handshake access overhead. In the 3-way handshake method, collisions occur due to RTS packet collisions. The initial random access success is modeled as a geometric distribution event, with an expected value of $\frac{1}{P_{\rm success}}$, indicating that an average of $\frac{1}{P_{\rm success}}$ attempts are needed to achieve successful access, corresponding to $\frac{1}{P_{\rm success}}-1$ collision events. Thus, the overhead of the 3-way handshake is as shown in (1). In contrast, the receiver-initiated 1-way handshake does not incur collision retransmission overhead, so the overhead is $O_{1\text{-way}}=T_{\rm CTS}+T_P$. Here, $T_{\rm RTS}$, $T_{\rm CTA}$, and $T_{\rm CTS}$ denote the transmission delays of the RTS, CTA, and CTS control messages, respectively, and T_p represents the propagation delay. The term $T_{\rm RTS}+T_{\rm CTS}+2T_p$ corresponds to the timeout duration for random access. If the terminal does not receive a response after transmitting data within this timeout period, it is assumed that a collision has occurred and the packet is retransmitted.

4.3 Delay of MAC mechanisms

Similar to the initial random handshake access, successful data packet transmission under random MAC mechanisms is also a geometric distribution event. The expected value is $\frac{1}{P_{\text{success}}}$, indicating that an

average of $\frac{1}{P_{\text{success}}}$ attempts are needed for successful transmission, corresponding to $\frac{1}{P_{\text{success}}} - 1$ collision

Thus, the packet transmission delay for the Aloha mechanism is

$$T_{\text{Aloha}} = \frac{T_{\text{data}} + T_P}{P_{\text{success,Aloha}}} + T_{\text{ACK}} + T_P. \tag{10}$$

The packet transmission delay for the S-Aloha mechanism is

$$T_{\text{S-Aloha}} = \frac{T_{\text{data}} + T_P}{P_{\text{success S-Aloha}}} + T_{\text{ACK}} + T_P, \tag{11}$$

where $T_{\rm data}$ is the transmission delay of the data packet, $P_{\rm success,Aloha}$ represents the successful transmission sion probability of the Aloha mechanism, $P_{\text{success,S-Aloha}}$ represents the successful transmission probability of the S-Aloha mechanism.

The TDMA packet transmission delay is modeled and analyzed using the M/D/1 queuing model. In an M/D/1 queue, the average queuing delay for a single packet can be calculated using the Pollaczek-Khinchine (P-K) formula, denoted as

$$T_{\text{queue}} = \frac{\rho}{2\mu(1-\rho)} = \frac{GT_{\text{data}}^2}{2(1-GT_{\text{data}})},\tag{12}$$

where the system utilization is $\rho = \frac{G}{\mu}$ and the service rate is $\mu = \frac{1}{T_{\text{data}}}$. Thus, the total transmission delay for a single TDMA packet is

$$T_{\text{TDMA}} = \frac{GT_{\text{data}}^2}{2(1 - GT_{\text{data}})} + T_{\text{data}} \cdot (1 + \text{PER}) + T_{\text{ACK}} + 2T_P.$$
 (13)

It should be noted that in the standard M/D/1 queuing model, it is assumed that the service time is fixed and every timeslot is utilized, meaning no idle slots. However, in practical TDMA systems, there may be idle timeslots when no terminals have data to send, which reduces the slot utilization rate and requires adjustments to the model by modifying the queue's service rate.

The packet arrivals at the terminals follow a Poisson process. The idle probability is $P_i = e^{-G}$, representing the probability that no data is transmitted in a given timeslot, and the TDMA timeslot utilization is $1 - P_i$. Since the standard M/D/1 model assumes that each timeslot transmits data, while actual TDMA may waste some slots, the corrected queue service rate is $\mu' = \frac{(1-P_i)}{T_{data}}$.

Substituting into the queuing delay formula gives

$$T_{\text{queue}} = \frac{GT_{\text{data}}^2}{2(1 - P_i)\left[(1 - P_i) - GT_{\text{data}}\right]}.$$
 (14)

Thus, the total transmission delay for each TDMA packet is $T_{\text{TDMA}} = T_{\text{queue}} + T_{\text{data}} \cdot (1 + \text{PER}) + T_{\text{data}} \cdot (1 + \text{PER})$ $T_{ACK} + 2T_P$.

Throughput of adaptive MAC scheme

The throughput is calculated as $S = \frac{L_{\text{total}}}{T_{\text{total}}}$, where L_{total} denotes the total amount of transmitted data, and T_{total} represents the total delay, including both handshake delay and packet transmission delay. Based on the above modeling process, the throughput expressions of different MAC mechanisms can be obtained as follows.

For the 3way-TDMA mechanism:

$$S_{3\text{way-TDMA}} = \frac{L_{\text{total}}}{T_{\text{total}}} = \frac{L_{\text{total}}}{O_{3\text{-way}} + T_{\text{frame}}}$$

$$= \left\{ N \cdot (1 - e^{-GN}) \cdot r \cdot T_{\text{slot}} \cdot (1 - \text{PER}) \right\} / \left\{ \left(\frac{1}{Ge^{-2G}} - 1 \right) \cdot (T_{\text{RTS}} + T_{\text{CTS}} + 2T_p) + (T_{\text{CTA}} + T_{\text{RTS}} + T_{\text{CTS}} + 3T_p) + N \cdot (1 - e^{-GN}) \cdot (T_{\text{slot}} + T_p + T_{\text{ACK}}) + T_p \right\}. \tag{15}$$

For the 1way-TDMA mechanism:

$$S_{1\text{way-TDMA}} = \frac{L_{\text{total}}}{T_{\text{total}}} = \frac{L_{\text{total}}}{O_{1\text{-way}} + T_{\text{frame}}}$$

$$= \frac{N \cdot (1 - e^{-GN}) \cdot r \cdot T_{\text{slot}} \cdot (1 - \text{PER})}{(T_{\text{CTS}} + T_p) + N \cdot (T_{\text{slot}} + T_p + T_{\text{ACK}}) + T_p}.$$
(16)

For the 1way-S-Aloha mechanism:

$$S_{1\text{way-S-Aloha}} = \frac{L_{\text{total}}}{T_{\text{total}}} = \frac{L_{\text{total}}}{O_{1\text{-way}} + T_{\text{S-Aloha}}}$$

$$= \frac{r \cdot T_{\text{slot}}}{(T_{\text{CTS}} + T_p) + \frac{(T_{\text{slot}} + T_p)}{G_{\text{C}} - T_{\text{C}} + T_p)} + T_{\text{ACK}} + T_p}.$$
(17)

For the 1way-Aloha mechanism:

$$S_{1\text{way-Aloha}} = \frac{L_{\text{total}}}{T_{\text{total}}} = \frac{L_{\text{total}}}{O_{1\text{-way}} + T_{\text{Aloha}}}$$

$$= \frac{r \cdot T_{\text{slot}}}{(T_{\text{CTS}} + T_p) + \frac{(T_{\text{slot}} + T_p)}{Ge^{-2G} \cdot (1 - \text{PER})} + T_{\text{ACK}} + T_p}.$$
(18)

The MCTA-MAC dynamically adjusts the THz beamwidth θ in each transmission cycle. According to the throughput model $S(m, G(\theta))$, the optimal handshake mechanism and MAC type are selected under different load and channel conditions. Meanwhile, based on network load and packet size, the frame length is adaptively adjusted and continuous timeslot windows are allocated to each terminal, enabling pipelined multi-packet transmission and reducing handshake overhead. Based on the selection of different mechanisms, the expressions of the adaptive MAC throughput can be derived as follows.

When the 3-way handshake and TDMA mechanism are selected, the throughput of the adaptive MAC is

$$S_{\text{Adaptive, 3way-TDMA}} = \frac{L_{\text{total}}}{T_{\text{total}}} = \frac{L_{\text{total}}}{O_{3\text{-way}} + T_{\text{frame}}}$$

$$= \left\{ N \cdot (1 - e^{-GN}) \cdot r \cdot T_{\text{slot}} \cdot (1 - \text{PER}) \right\} / \left\{ \left(\frac{1}{Ge^{-2G}} - 1 \right) \right.$$

$$\cdot \left(T_{\text{RTS}} + T_{\text{CTS}} + 2T_p \right) + \left(T_{\text{CTA}} + T_{\text{RTS}} + T_{\text{CTS}} + 3T_p \right) + N \cdot (1 - e^{-GN}) \cdot T_{\text{slot}} \right.$$

$$\left. + \frac{r \cdot T_{\text{slot}} \cdot N \cdot (1 - e^{-GN})}{L_{\text{req}}} \cdot (T_p + T_{\text{ACK}}) + T_p \right\}. \tag{19}$$

When the 1-way handshake and TDMA mechanism are selected, the throughput of the adaptive MAC is

$$S_{\text{Adaptive, 1way-TDMA}} = \frac{L_{\text{total}}}{T_{\text{total}}} = \frac{L_{\text{total}}}{O_{\text{1-way}} + T_{\text{frame}}}$$

$$= \frac{N \cdot (1 - e^{-GN}) \cdot r \cdot T_{\text{slot}} \cdot (1 - \text{PER})}{(T_{\text{CTS}} + T_p) + N \cdot \left(T_{\text{slot}} + \frac{r \cdot T_{\text{slot}}}{L_{\text{req}}} \cdot (T_p + T_{\text{ACK}})\right) + T_p}.$$
(20)

When the 1-way handshake and S-Aloha mechanism are selected, the throughput of the adaptive MAC is

$$S_{\text{Adaptive},1\text{way-S-Aloha}} = \frac{L_{\text{total}}}{T_{\text{total}}} = \frac{L_{\text{total}}}{O_{1\text{-way}} + T_{\text{S-Aloha}}}$$

$$= \left\{ \frac{1}{1 - Ge^{-G} \cdot (1 - \text{PER})} \cdot r \cdot T_{\text{slot}} \right\} / \left\{ (T_{\text{CTS}} + T_p) + \left(\frac{1}{Ge^{-G} \cdot (1 - \text{PER})} - 1 \right) \cdot (T_{\text{slot}} + T_p) + \frac{1}{1 - Ge^{-G} \cdot (1 - \text{PER})} \cdot T_{\text{slot}} + T_{\text{ACK}} + 2T_p \right\}.$$

$$(21)$$

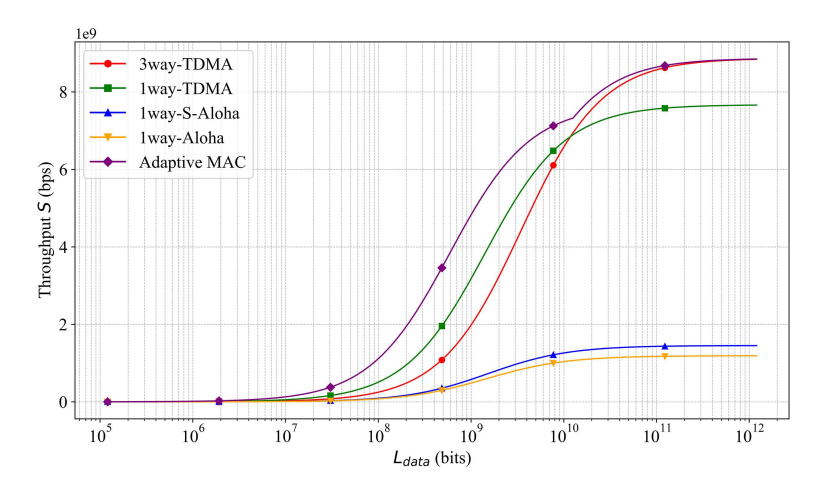


Figure 6 (Color online) Throughput performance curves of different MAC mechanisms under varying payload sizes.

Here, r denotes the link transmission rate, $T_{\rm slot}$ is the duration of a single timeslot, $L_{\rm req}$ is the data packet length, $T_{\rm RTS}$ and $T_{\rm CTS}$ are the transmission delays of RTS and CTS control messages, T_p is the propagation delay, $T_{\rm ACK}$ is the acknowledgment delay, N is the number of LEO satellites covered by the beam, G is the traffic load, and PER is the packet error rate.

5 Performance impact of STIN MAC mechanisms and adaptive capability analysis

Based on the previously constructed STIN MAC theoretical analysis model, this section analyzes the impact of multiple service transmission parameters, such as payload size, traffic load, the number of LEO terminals, and propagation delay, on the performance of MAC mechanisms. The analysis summarizes the laws governing the influence of these factors and reveals the impact of STIN communication characteristics (such as ultra-large bandwidth, narrow beams, and long propagation delay) on the mechanisms and performance of MAC schemes. The modeling and simulation results further compare the performance differences of adaptive MAC and traditional MAC mechanisms under multiple scenarios, providing theoretical support for mechanism optimization and multi-parameter configuration.

To analyze the potential performance upper bound of mechanism design, this paper adopts certain idealized assumptions regarding system parameters and mechanism implementation. For example, it is assumed that satellite terminals are equipped with high-gain phased array antennas, wideband RF frontends, and high-speed beam tracking capability. The delay of adaptive switching is ignored, and stable operation is assumed throughout the entire visibility window. These assumptions allow the analysis to eliminate the influence of hardware constraints on mechanism performance, thereby focusing on the adaptability and scheduling effectiveness of the mechanisms themselves.

5.1 Impact of transmission payload $L_{\rm data}$ on throughput S

 $L_{\rm data}$ denotes the payload size transmitted by a terminal after a successful channel access, excluding signaling overhead, with units in bits. Under fixed link budget conditions ($G=0.2,\ r=10$ Gbps, $T_{\rm RTS}=T_{\rm CTS}=T_{\rm CTA}=32$ ns, $T_{\rm ACK}=11.2$ ns, $T_p=0.11785$ s, PER=0.1131, and N=10), the impact of payload size $L_{\rm data}$ on throughput S is analyzed.

The model analysis results are shown in Figure 6. As $L_{\rm data}$ increases, the throughput of each MAC mechanism gradually approaches a stable value. In the small $L_{\rm data}$ region, signaling overhead accounts for a large proportion, leading to low utilization efficiency. In the medium region, the proportion of signaling overhead decreases, throughput utilization improves, and throughput increases significantly before stabilizing. For 3way-TDMA with handshake-based slot allocation, when $L_{\rm data} > 10^{10}$ bits, the additional signaling overhead leads to performance degradation, and throughput is surpassed by 1way-TDMA. Contention-based access mechanisms (1way-S-Aloha, 1way-Aloha) are limited by collision probability, and overall throughput is lower. Compared with traditional MAC mechanisms, MCTA-MAC achieves better performance across different payload ranges. In particular, MCTA-MAC dynamically

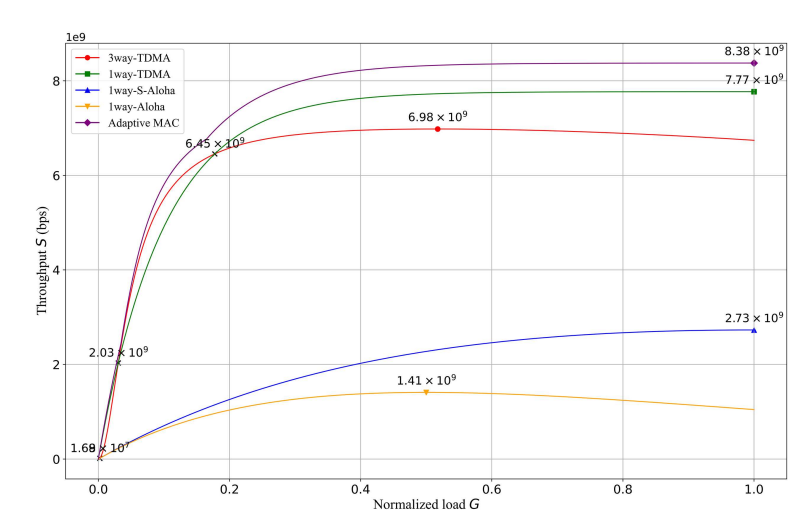


Figure 7 (Color online) Throughput performance curves of different MAC mechanisms under varying traffic loads.

adjusts handshake modes, adopting 1way-TDMA in the small payload region to reduce signaling overhead, and adopting 3way-TDMA in the large payload region to improve reliability. This allows the mechanism to adaptively adjust signaling overhead according to payload distribution, achieving smooth throughput evolution and improved utilization efficiency.

5.2 Impact of traffic load G on throughput S

Under fixed link budget and service parameters (r=10 Gbps, $T_{\rm RTS}=T_{\rm CTS}=T_{\rm CTA}=32$ ns, $T_{\rm ACK}=11.2$ ns, $T_p=0.11785$ s, PER = 0.1131, N=10, $L_{\rm data}=10^{10}$ bits), the impact of traffic load G on throughput S is analyzed.

The model analysis results are shown in Figure 7. As G increases, the throughput of each MAC mechanism first increases and then approaches saturation in the medium-to-high load region. The throughput of 3way-TDMA and 1way-Aloha decreases when traffic load becomes high due to the increase of signaling overhead and collisions. Compared with traditional mechanisms, MCTA-MAC shows performance advantages across different load regions. This mechanism can adaptively adjust signaling overhead and avoid excessive control overhead under light load, while also avoiding frequent collisions under heavy load. Through dynamic allocation of access resources, the mechanism realizes smooth throughput evolution, effectively improving utilization efficiency.

5.3 Impact of the number of LEO satellites N on throughput S

Under fixed link budget and service parameters (G = 0.2, r = 10 Gbps, $T_{\rm RTS} = T_{\rm CTS} = T_{\rm CTA} = 32$ ns, $T_{\rm ACK} = 11.2$ ns, $T_p = 0.11785$ s, PER = 0.1131, $L_{\rm data} = 10^{10}$ bits), the impact of the number of terminals N on throughput S is analyzed.

The model analysis results are shown in Figure 8. The throughput of TDMA-type mechanisms increases rapidly with the growth of N and then gradually approaches saturation. Random access mechanisms are not affected by N under a fixed G, and due to the high collision probability, their throughput curves remain constant and far lower than those of TDMA-type mechanisms. As N increases, the proportion of idle slots decreases, the advantage of dynamic allocation in 3way-TDMA gradually diminishes, and the performance of 1way-TDMA surpasses that of 3way-TDMA. MCTA-MAC maintains the highest performance across the entire range of terminal numbers, owing to its adaptive selection of low-overhead mechanisms to accelerate entry into the saturation region, and its switching to a more stable TDMA mode in multi-terminal scenarios. By combining frame length adaptation with continuous slot pipelined allocation, it effectively sustains link utilization and fairness.

5.4 Impact of propagation delay T_p on throughput S

The model parameters are set as G=0.2, $L_{\rm data}=10^8$ bits, r=10 Gbps, $T_{\rm RTS}=T_{\rm CTS}=T_{\rm CTA}=32$ ns, $T_{\rm ACK}=11.2$ ns, PER = 0.1131, and N=10, the impact of propagation delay T_p on throughput S is analyzed.

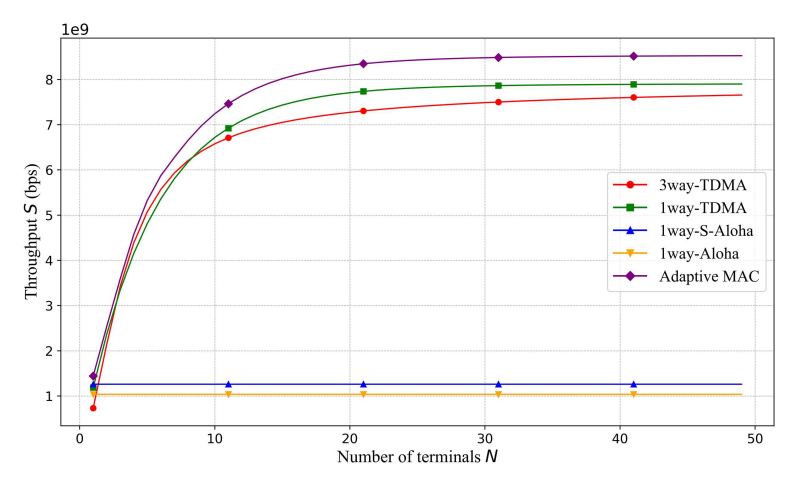


Figure 8 (Color online) Throughput performance curves of different MAC mechanisms under varying numbers of LEO satellites.

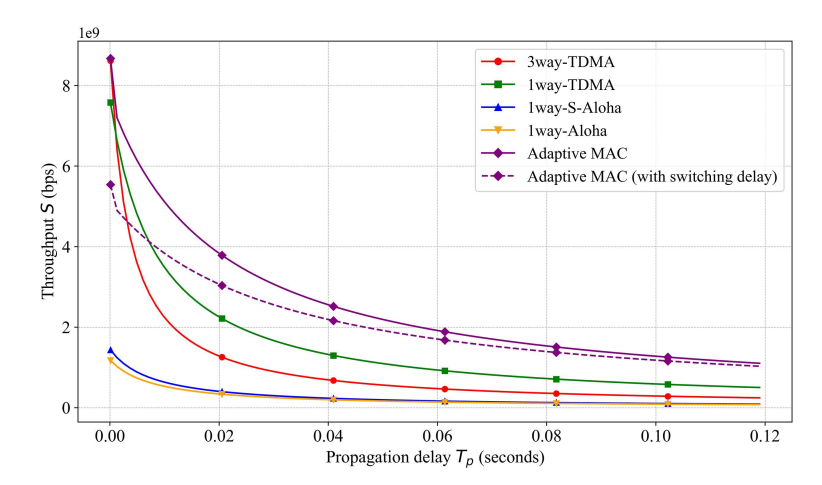


Figure 9 (Color online) Throughput performance curves of different MAC mechanisms under varying delay overheads.

The model analysis results are shown in Figure 9. As T_p increases, the throughput of each MAC mechanism decreases, with the decline being more obvious when T_p is large. For $T_p > 1$ ms, the advantage of 3way-TDMA with dynamic slot allocation diminishes due to the additional signaling overhead brought by propagation delay, which significantly reduces effective transmission efficiency. Contention-based mechanisms (1way-S-Aloha, 1way-Aloha) are more severely affected, and overall throughput decreases significantly. MCTA-MAC shows robustness across different propagation delay scales, maintaining advantages by adaptively controlling signaling and slot allocation, reducing redundant retransmissions, and alleviating the efficiency loss caused by long RTT.

In addition, the impact of MAC parameter switching delay is considered. Assuming an average MAC switching delay of 40 ms, throughput decreases slightly, with the decline within 0.5%. This does not affect the overall performance advantage of the mechanism. In future systems, signaling channels can be introduced to separate the control plane from the data plane, thereby reducing the delay cost of adaptive switching and further improving efficiency.

5.5 Theoretical performance surface

This subsection analyzes the joint impact of normalized traffic load G and service payload size $L_{\rm data}$ on throughput S. By calculating the throughput distribution of different MAC mechanisms within the G- $L_{\rm data}$ two-dimensional parameter space, the interaction effects of these two factors and their performance differences under different mechanisms are further revealed. This provides a more comprehensive understanding of the impact of STIN communication characteristics on MAC performance. The model parameters are set as follows, r=10 Gbps, $T_{\rm RTS}=T_{\rm CTS}=T_{\rm CTA}=32$ ns, $T_{\rm ACK}=11.2$ ns, $T_p=0.11785$ s, N=10, PER = 0.1131. The normalized traffic load G ranges within $G\in[0.01,1]$, and the

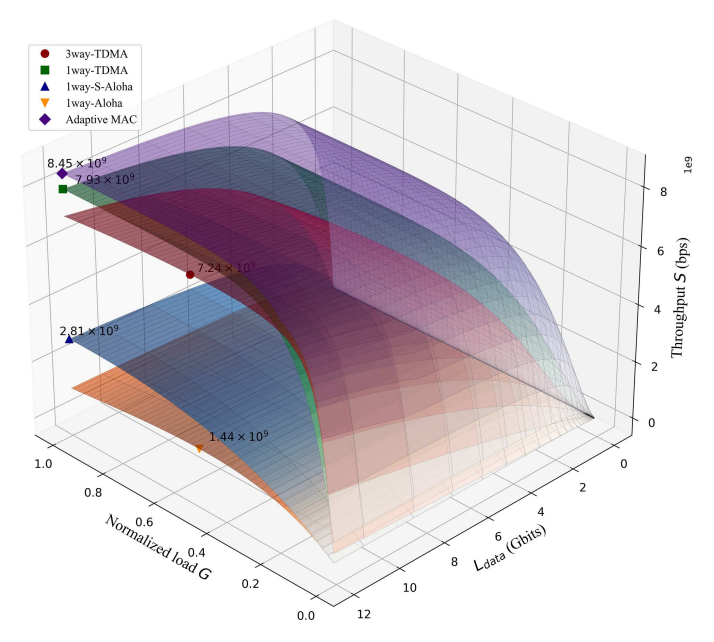


Figure 10 (Color online) Throughput performance surfaces of different MAC mechanisms under normalized load G and payload size $L_{\rm data}$. The results based on the theoretical model show that the adaptive MAC consistently achieves higher throughput under diverse load and packet size conditions, exhibiting clear advantages over traditional mechanisms (3way-TDMA, 1way-TDMA, 1way-S-Aloha, 1way-Aloha).

payload size ranges within $L_{\rm data} \in [1.2 \times 10^2, 1.0 \times 10^{10}]$ bits.

The theoretical performance surface is shown in Figure 10. From the surface results, all mechanisms exhibit a rapid increase in throughput within the low-G region, followed by a gradual saturation in the medium-to-high load region. In the low- $L_{\rm data}$ region, frequent signaling dominates, single-packet throughput is low, and all mechanisms show relatively low performance. As $L_{\rm data}$ increases, the signaling overhead ratio decreases, throughput grows rapidly, and performance improves. When $L_{\rm data}$ approaches the upper bound, throughput is constrained by PER, and all five mechanisms gradually converge. The difference between the two TDMA surfaces reflects the trade-off between handshake and scheduling. 3way-TDMA falls behind 1way-TDMA in the small-L and low-G region due to the additional handshake overhead, but as G increases and L becomes larger, the two mechanisms converge in performance owing to the stronger slot coordination capability and lower collision risk of 3way-TDMA. The overall rise of the surfaces of contention-based mechanisms is constrained by the combined effects of collision probability and PER, making it difficult to achieve gains comparable to TDMA as G increases. Across the entire parameter space, MCTA-MAC achieves the best performance among all mechanisms.

It can be seen that in the high-bandwidth THz scenario, sufficiently increasing the effective transmission payload $L_{\rm data}$ can significantly reduce the G threshold required to reach the saturation region. Moreover, the throughput gains along both dimensions exhibit clear diminishing returns-the closer to the saturation region, the more limited the improvement from further increasing G or L. By adaptively adjusting the MAC mode, selecting low-overhead handshake methods and MAC strategies, the proportion of idle time slots caused by round-trip interactions can be reduced. Through continuous time slot window allocation, the throughput dilution effect caused by propagation delay can be alleviated, and the overhead ratio of long RTTs can be effectively flattened, thereby significantly improving the performance of MAC mechanisms.

In summary, the modeling analysis quantitatively reveals the coupling mechanism between the communication characteristics of STIN (ultra-large bandwidth, narrow beams, and long RTT) and MAC design factors (mechanism switching, handshake selection, and time slot allocation), and verifies that MCTA-MAC possesses comprehensive advantages including higher peak throughput, earlier entry into saturation, and greater stability in the saturation region.

6 Simulation and analysis

6.1 Simulation cases and parameter design

This chapter focuses on a typical communication scenario between GEO satellites and LEO constellations in the STIN. A simulation case that conforms to realistic operational characteristics is designed to deeply analyze the performance of the proposed adaptive MAC mechanism under practical conditions, and to validate the accuracy and applicability of the theoretical model proposed earlier. In the simulation scenario, the GEO satellite is positioned at 110.5°E in the geostationary orbit, equipped with a multibeam phased array antenna. By utilizing a large-scale antenna array, multiple narrow beams are formed, enabling simultaneous access to multiple LEO satellites within the coverage area. The LEO constellation adopts the STARLINK configuration, consisting of approximately 8100 in-orbit satellites at an altitude of about 550 km, distributed across more than 72 orbital planes.

In this paper, different MAC mechanisms are compared under the same network topology, link conditions, and traffic arrival characteristics. Traffic flows are generated according to a Poisson arrival model, and each satellite node in the simulation scenario maintains an independent packet queue. In the ALOHA mechanism, packets are transmitted with random delays, if multiple nodes transmit within the same time window, a collision occurs and the packets are discarded. The 1way-TDMA mechanism allocates resources according to a fixed slot table, avoiding collisions but lacking dynamic adjustment. The 3way-TDMA mechanism introduces a 3-way handshake on top of TDMA, enabling slot adjustment according to queue and link status. The adaptive MAC mechanism switches among the above mechanisms according to the current state. The simulation platform is independently developed in Python, based on a discrete-event driven framework, and implements modules for packet generation, protocol scheduling, collision detection, and performance statistics. The platform allows the configuration of protocol type, traffic intensity, and link parameters, enabling statistical analysis of throughput and delay of different mechanisms under varying conditions. By averaging the results of multiple independent runs, the reproducibility of results and fairness of comparisons are ensured.

Based on this setup, an STIN communication simulation model considering link quality fluctuations is constructed. A Monte Carlo simulation method is used to perform multiple independent experiments to ensure statistical stability of the results, and to quantitatively evaluate the performance advantages of the adaptive MAC mechanism under practical conditions as well as its robustness under varying link scenarios. The relevant simulation parameters are listed in Table 1, the link budget parameters (such as THz carrier frequency, beam gain, and transmission distance) are set for theoretical evaluation, aiming to explore the potential boundaries of terahertz communication mechanisms in highly dynamic scenarios. Therefore, some parameter settings are relatively idealized and exceed the capabilities of existing systems [27]. For example, the assumed antenna gain is above 50 dBi, and the link distance reaches up to 36000 km, which is beyond the actual capacity of current terahertz communication devices. Accordingly, we have pointed out that system-level implementation still depends on the future development of high-power THz amplifiers, high-sensitivity receivers, and high-speed beam scheduling mechanisms.

6.2 Simulation performance surface

Under the constructed GEO-LEO satellite terahertz communication simulation scenario, the performance of the proposed adaptive MAC mechanism and several typical fixed MAC mechanisms (1way-TDMA, 3way-TDMA, 1way-S-Aloha, 1way-Aloha) is evaluated in the two-dimensional parameter space of G-L. In the simulation, the normalized traffic load G ranges within [0,1], and the payload size L ranges within $[1.2 \times 10^5, 1.2 \times 10^{10}]$ bits. Other link parameters remain consistent with the configuration used in the theoretical analysis.

In this paper, throughput in the theoretical model is defined as the amount of effective data successfully transmitted per unit time, while the total delay includes both data transmission time and protocol overhead, such as handshake, acknowledgment, propagation delay, and guard intervals. In the simulations, throughput is obtained by statistical averaging over multiple independent experiments. For each experiment, the ratio of the total successfully transmitted data to the corresponding total delay is calculated, and then the results of multiple experiments are averaged. This method ensures the physical consistency between the simulation calculations and the theoretical definition.

The simulation results are shown in Figure 11, the throughput S of each MAC mechanism exhibits trends consistent with the theoretical predictions as G and L vary jointly. A typical pattern of slow

Table 1 Simulation parameters.

Parameter	Symbol	Formula/description	Reference value	Unit
Transmitter parameters				
Operating frequency	f	THz band selection	0.3	THz
Transmission power	P_t	Power amplifier output	40	$_{ m dBm}$
Transmitter antenna gain	G_t	$G \approx 10 \log_{10} \left(\frac{4\pi}{\theta^2} \right)$	72.26	$_{ m dBi}$
Single beamwidth	θ	$G \approx 10 \log_{10} \left(\frac{4\pi}{\theta^2} \right)$	0.05	0
Number of beams	$N_{ m beam}$	Number of synthesized beams	100	_
Propagation path parameters				
GEO-LEO distance	d	Average distance	36000	km
Free-space path loss	L_f	$L_f = 20 \log \left(\frac{4\pi df}{c} \right)$	233.11	dB
Atmospheric loss	$L_{ m atm}$	Near-vacuum environment	0	dB
Receiver parameters				
Receiver antenna gain	G_r	Same as transmitter gain formula	72.26	dBi
Transmission rate	r	Target data rate defined by the system design	10	Gbps
System temperature	$T_{ m sys}$	Low-noise receiver	500	K
Noise power	N_p	$N_p = 10\log\left(k_B T_{\rm sys} B\right) + 30$	-83.6	dBm
Demodulation threshold	${\rm SNR_{\min}}$	$64QAM, BER \approx 10^{-6}$	20	dB
MAC layer and simulation contro	l parameters	3		
Number of simulation timeslots	$N_{ m slot}$	Number of simulated timeslots	1000	_
Payload size	L_{data}	Size of a single payload size transmitted	10^{10}	bits
Control packet size	$L_{\rm control}$	Size of a single control packet	320	bits
ACK message size	L_{ACK}	Size of a single ACK message	112	bits
Packet error rate	PER	Probability of packet errors	0.113	_
Probability of LEO transmission	q	Probability of LEO transmitting in one timeslot	0.02	_

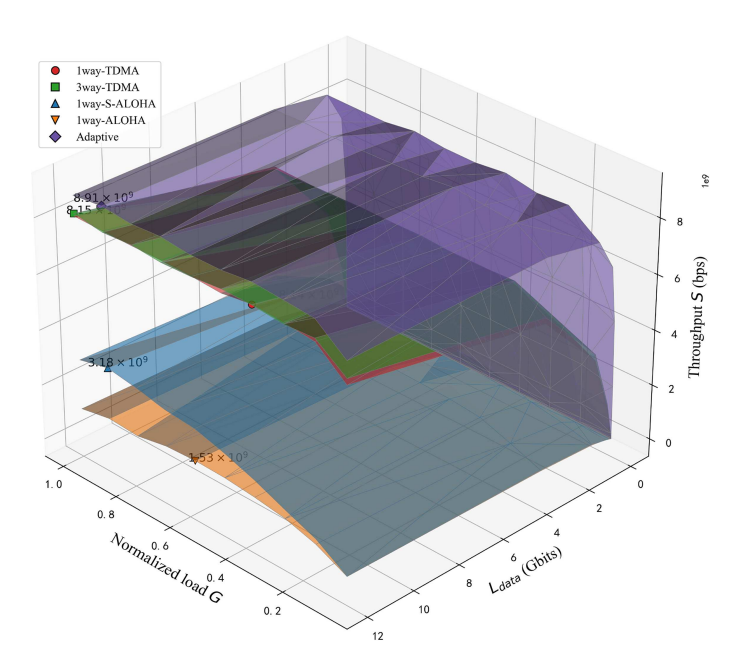


Figure 11 (Color online) Throughput performance of different MAC mechanisms in the simulation case under normalized load G and payload size $L_{\rm data}$. The simulation results validate the accuracy of the constructed STIN MAC theoretical analysis model as well as its applicability to practical scenarios.

increase in the low-value region, rapid growth in the middle region, and eventual saturation is observed. Among them, MCTA-MAC consistently outperforms other fixed mechanisms across the entire parameter space. These results validate the accuracy of the proposed STIN MAC theoretical analysis model as well as its applicability to practical scenarios, further confirming the performance advantages and robustness of MCTA-MAC under varying parameter conditions.

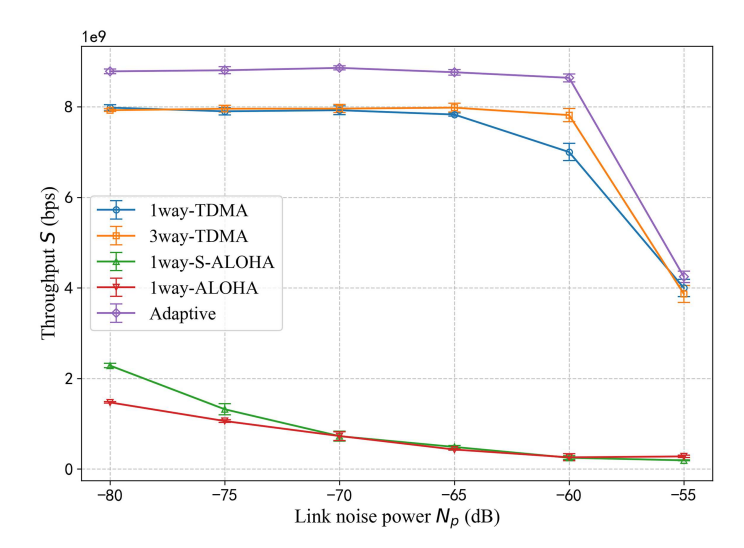


Figure 12 (Color online) Comparison of throughput performance of different MAC mechanisms under varying link noise power. The simulation results show that the MCTA-MAC consistently maintains the highest throughput, demonstrating superior robustness against interference.

6.3 Performance analysis of MCTA-MAC under link quality fluctuations

In the simulation scenario, the GEO satellite uses a multi-beam phased array antenna and forms multiple narrow beams through a large number of array elements to achieve regional coverage. Based on the reception threshold exceeding the access threshold, the average link success probability can be estimated, from which the THz beamwidth range can be calculated. The THz beamwidth affects the number of LEO satellites covered, and thus determines the traffic load G. When link quality fluctuates, MCTA-MAC dynamically adjusts the beamwidth based on real-time link conditions, adapts the access mechanism accordingly, and selects the optimal MAC type to maximize throughput under varying link quality and load conditions.

Based on this simulation scenario, we construct an STIN communication simulation model considering link quality fluctuations. A large number of independent Monte Carlo simulations are performed to evaluate the performance advantage and robustness of the proposed MCTA-MAC mechanism under different link quality conditions, the simulation results are illustrated in Figure 12.

When the link noise power varies from -80 to -55 dB, the corresponding THz beamwidth changes from 9.55° to 2.26° . Using TLE data of GEO and LEO satellites, the number of visible LEO satellites is calculated. As the visible LEO count changes from 297 to 17, the probability of any given LEO sending a data packet is 0.0015, and the corresponding G value increases from 0.003 to 0.456.

From the simulation results, it can be observed that due to the dynamic adjustment capability of the MCTA-MAC mechanism, it maintains the best performance under fluctuating link quality. Based on the Monte Carlo simulations, although fluctuations exist in each sampling trajectory, the overall performance trend remains clear. When link noise power is -60 dB (low load), the throughput of MCTA-MAC improves by 27% over 1way-TDMA and by 12% over 3way-TDMA, when link noise power is -74 dB (high load), the improvement over 3way-TDMA and 1way-TDMA is 12%, showing that MCTA-MAC can maintain high adaptability and robustness. It matches the characteristics of THz transmission, enabling effective communication even under link quality degradation and high-load conditions. These simulation results are consistent with the previously proposed theoretical model, further validating the correctness and applicability of the proposed analytical approach.

7 Conclusion

This paper focuses on the high-performance communication requirements of space terahertz information networks. Addressing the limitations of existing MAC protocols that fail to fully consider THz characteristics and are difficult to adapt to complex space environments, this study investigates an adaptive MAC mechanism for STIN. By constructing a STIN MAC performance analysis framework based on queuing theory and geometric probability models, the work systematically reveals the impact of key STIN

communication parameters (such as beamwidth, ultra-wide bandwidth, and long propagation delay) on throughput performance and channel scheduling efficiency, and clarifies the trade-off between random access and fixed allocation mechanisms in STIN.

On this theoretical basis, a multi-dimensional cooperative adaptive STIN MAC scheme is proposed. In each transmission cycle, the scheme jointly considers physical-layer beam gain and line-of-sight coverage, link-layer load and signal-to-noise ratio, and network-layer task scheduling requirements, thereby enabling dynamic adjustment of beamwidth, handshake method, MAC strategy, and slot allocation. This ensures alignment with the high-speed transmission capability of THz links and improves link resource utilization. Simulation experiments are conducted with GEO satellites and LEO constellations as representative cases. The results verify the accuracy and generality of the theoretical model and demonstrate that the proposed adaptive MAC mechanism exhibits stronger robustness and adaptability in complex space environments, significantly enhancing communication efficiency in STIN. The study not only fills the gap in theoretical analysis of STIN MAC performance but also provides a feasible methodological reference for protocol design in future high-speed terahertz satellite communication networks.

Acknowledgements This work was supported by National Natural Science Foundation of China (Grant No. 62341128).

References

- 1 Chen Z, Ma X, Zhang B, et al. A survey on terahertz communications. China Commun, 2019, 16: 1-35
- 2 Hao Q, Zhou D, Sheng M, et al. Tiered clustering-based management architecture in mega-satellite networks. Sci China Inf Sci, 2024, 67: 152301
- 3 Akyildiz I F, Han C, Hu Z, et al. Terahertz band communication: an old problem revisited and research directions for the next decade. IEEE Trans Commun, 2022, 70: 4250–4285
- 4 He Y Z, Ma C S, Yin H. Measuring the radiation hardness of terahertz devices for space applications. Commun Phys, 2024, 7: 362
- 5 Do H, Cho S, Park J, et al. Terahertz line-of-sight MIMO communication: theory and practical challenges. IEEE Commun Mag, 2021, 59: 104–109
- 6 Wu Y P, Xu M, Zhai G T, et al. Physical layer signal processing for XR communications and systems. Sci China Inf Sci, 2024, 67: 221301
- 7 Ghafoor S, Boujnah N, Rehmani M H, et al. MAC protocols for terahertz communication: a comprehensive survey. IEEE Commun Surv Tut, 2020, 22: 2236–2282
- 8 3GPP. Study on New Radio (NR) to Support Non-terrestrial Networks. TR 38.811, 2020
- 9 ITU-R. IMT traffic estimates for the years 2020 to 2030. Recommendation M.2460, 2019
- 10 Chen Y, Li Y, Han C, et al. Channel measurement and ray-tracing-statistical hybrid modeling for low-terahertz indoor communications. IEEE Trans Wireless Commun, 2021, 20: 8163-8176
- 11 Ma S, He Y, et al. Channel modeling techniques for space terahertz communication (in Chinese). Applied Laser, 2024, 44: 123–138
- 12 Chen W, Li L, Chen Z, et al. Coverage modeling and analysis for outdoor THz networks with blockage and molecular absorption. IEEE Wireless Commun Lett, 2021, 10: 1028–1031
- 13 Wu Y, Kokkoniemi J, Han C, et al. Interference and coverage analysis for terahertz networks with indoor blockage effects and line-of-sight access point association. IEEE Trans Wireless Commun, 2020, 20: 1472–1486
- 14 Busari S A, Huq K M S, Mumtaz S, et al. Generalized hybrid beamforming for vehicular connectivity using THz massive MIMO. IEEE Trans Veh Technol, 2019, 68: 8372–8383
- 15 He Y, Ma C. Analysis of the effect of antenna pointing error caused by satellite perturbation on space terahertz communication. Appl Sci, 2022, 12: 10772
- 16 Yuan H, Yang N, Ding X, et al. Cluster-based multi-carrier hybrid beamforming for massive device terahertz communications. IEEE Trans Commun, 2022, 70: 3407–3420
- 17 Xia Q, Hossain Z, Medley M, et al. A link-layer synchronization and medium access control protocol for terahertz-band communication networks. IEEE Trans Mobile Comput, 2019, 20: 2–18
- 18 Xia Q, Jornet J M. Cross-layer analysis of optimal relaying strategies for terahertz-band communication networks. In: Proceedings of the 13th International Conference on Wireless and Mobile Computing, Networking and Communications (WiMob), 2017. 1–8
- 19 Lin C, Li G Y. Adaptive beamforming with resource allocation for distance-aware multi-user indoor terahertz communications. IEEE Trans Commun, 2015, 63: 2985–2995
- 20 Han C, Tong W, Yao X W. MA-ADM: a memory-assisted angular-division-multiplexing MAC protocol in Terahertz communication networks. Nano Commun Netws, 2017, 13: 51–59
- 21 Morales D, Jornet J M. ADAPT: an adaptive directional antenna protocol for medium access control in terahertz communication networks. Ad Hoc Netws, 2021, 119: 102540
- 22 Wang D, Mei W, Chen Z, et al. Performance analysis and reflection optimization for wideband THZ double-IRS aided wireless communications. In: Proceedings of IEEE International Conference on Communications, 2024. 2519–2524
- 23 He L, Hu F, Chu Z, et al. Intelligent terahertz medium access control (MAC) for highly dynamic airborne networks. IEEE Trans Aerosp Electron Syst, 2022, 59: 2494–2512
- 24 Absaruddin M, Ghafoor S, Rehmani M H. Beamwidth trade-offs analysis of THZ MAC protocols for wireless data center. In: Proceedings of International Wireless Communications and Mobile Computing (IWCMC), 2024. 1345–1350
- 25 Absaruddin M, Ghafoor S, Rehmani M H. Dynamic beamwidth selection-based THZ MAC protocol for wireless data center networks. In: Proceedings of the 20th International Conference on Wireless and Mobile Computing, Networking and Communications (WiMob), 2024. 526–531
- 26 Chen W, Li L, Ning B, et al. Sensing resource allocation for enlarging the coverage range of ISAC-based terahertz network. In: Proceedings of IEEE Global Communications Conference, 2023. 3639–3644
- 27 He Y, Ma C. Research on frequency selection method for spatial terahertz communication under multiple constraints. In: Proceedings of the 22nd International Conference on Communication Technology (ICCT), 2022. 774–781